Distribution of this document is unlimited.

GENERAL DYNAMICS
ASTRONAUTICS

Best
Available
Copy

PRIVATE DATA

REPORT NO. ERR-AN-100

DATE 28 Nov. 1961

NO. OF PAGES

CLASSIFICATION CHANGED TO:
UNCLASSIFIED
AUTHORIZED BY: ~~DD 254~~ DATE AUG 8 '68
CONTRACT NO. Per M Dublin
RECLASSIFIED BY: [illegible]
DEPT. 130-1 DATE 4-11-68
R. J. COOK, SECURITY OFFICER
CONVAIR DIVISION OF GENERAL DYNAMICS

CONVAIR | ASTRONAUTICS

CONVAIR DIVISION OF GENERAL DYNAMICS CORPORATION

HYPERSONIC UTILITY GLIDER

THERMODYNAMIC ANALYSIS

[redacted]

Distribution of this document is unlimited.

AD 672194

C. G. Forsythe

PREPARED BY C. P. Melfi, F. D. Postula
C. G. Forsythe, C. P. Melfi,
F. D. Postula

CHECKED BY J C Ballinger
J. C. Ballinger

APPROVED BY W B Mitchell
W. B. Mitchell
Chief of Aerophysics

APPROVED BY W F Radcliffe
W. F. Radcliffe
Chief Development Engineer

Removal of Private markings authorized by Patent Dept 3/19/68
W F Martin

REVISIONS

NO.	DATE	BY	CHANGE	PAGES AFFECTED

PRIVATE DATA

FORM NO. A-700-1

FOREWORD

The purpose of this memorandum is to present a preliminary heat shield and weight analysis for the six-man Multi-Mission Utility Glider under study by General Dynamics/Astronautics.

TABLE OF CONTENTS

LIST OF TABLES

LIST OF ILLUSTRATIONS

LIST OF ILLUSTRATIONS (Cont)

SUMMARY

Heating analyses indicated an ablative type heat shield was necessary for the stagnation regions of the Utility Glider, i.e. the nose cap, leading edges and bottom surface; while the cooler upper surface was adequately protected by a radiative type heat shield.

Four configurations of the Multi-Mission Re-entry Vehicle (or Utility Glider) were analyzed for total heat shield weight. Whereas all four configurations are delta wing glide vehicles, three are very similar in shape while the fourth has a much flater upper surface and a radically curved bottom surface. Primary difference in the first three configurations is the seating arrangement of the occupants. The total heat shield weight for the first three configurations varied from 3616 to 3712 pounds while the fourth configurations heat shield weight was found to be 3179 pounds.

INTRODUCTION

The re-entry heating studies were based on three trajectories, a lifting undershoot, a drag overshoot and a coast trajectory. Total vehicle heat shield weight was based on the summation of the weight of the varying types and thicknesses of the heat shields at six vehicle locations: (1) Nose Cap, (2) Swept wing leading edges, (3) Tail fins, (4) Bottom Surface, (5) Upper Surface, and (6) Viewing port. In all locations the drag overshoot trajectory produced the greatest total heat input and consequently the most severe heating on the heat shield materials; therefore, all heat shield designs at the above six locations were based on the drag overshoot trajectory.

DISCUSSION AND RESULTS

A. Aerodynamic Heating

Since the vehicles of interest in our discussion re-enter at satellite and escape velocity, they are exposed to very high temperature air, the properties of which deviate from an ideal gas. At velocities of about 3000 fps, the vibrational modes are excited; then dissociation starts for oxygen at about 7000 fps and for nitrogen at about 15,000 fps. The reference enthalpy method has been successful in predicting the heating for satellite re-entry where these chemical reactions are of major importance (Reference 1). At escape velocity the important reaction is the ionization of the oxygen and nitrogen atoms. Although there is little aerodynamic heating data at these conditions, it is believed that the reference enthalpy method will be useful in predicting the aerodynamic heating from an engineering standpoint. The convective heating used through this analysis was based on continuum flow. The overall effect of convective heating in the free-molecular and slip-flow regimes is in general of little concern for ICBM and ballistic type re-entry vehicles. However, it is possible that for high lift, long glide time vehicles or satellites the difference between vehicle heating calculated from the slip-flow and continuum regimes may become significant, and will be considered in more detail in the continuing study.

Additional heat input to the vehicle is experienced by radiation from the glowing hot gas cap created by the nose cone and shock wave. The radiation from the gas cap surrounding the nose of a blunt vehicle re-entering at escape velocity may become a significant portion of the total heat input. The method used to compute the radiative heat flux to the stagnation zones from the gas cap is from Kivel (Reference 2) and assumes a equilibrium hot gas. When non-equilibrium conditions occur, however, the resulting radiation will generally be higher than equilibrium radiation. It has been shown (Reference 3) that non-equilibrium radiation can be as much as an order of magnitude higher than equilibrium conditions. Fortunately, non-equlibrium conditions exist generally at high altitudes where the magnitude of the radiation is itself low. For this analysis the assumption of equilibrium conditions does not contribute any significant error to the calculations.

B. Entry Corridor

Three trajectory conditions describe the entry limitations for the Multi-Mission Re-entry Vehicle. First is the drag overshoot boundary for which the velocity remains above circular velocity during the initial penetration but is reduced sufficiently to allow entry after a skip-out coast phase. This boundary is shown in Figure 1. The second is the lifting undershoot which allows a steeper entry and is shown in Figure 2. Figure 3 shows the third boundary condition, the coast phase from circular velocity. In these analyses, the addition of one of the first two boundary trajectories to the coast phase constitutes a complete re-entry flight trajectory. It might be noted that the altitude and velocity of Figures 1 and 2 do not precisely match those of Figure 3. In the analyses the curves were combined by a step change to represent a continuous flight. The small discontinuity produced in the altitude and velocity at this point in the trajectory did not cause a large discontinuity in the temperature history curves.

C. Configurations

Heating and weight analyses were performed on four configurations of the Multi-Mission Re-entry Vehicle. The four were configurations 2A, 1B, 2B and 3B. Configuration 2A, shown in Figure 4, is representative of configurations 2B and 3B except for the seating arrangement of the six passengers of the vehicle. Configuration 2A has two men in front side by side and four men side by side in the rear portion of the cabin volume. . Configuration 2B has three-three arrangement while configuration 3B has a two-two-two seating arrangement. Configuration 1B, shown in Figure 5, is somewhat different from the other configurations in that it has a flat upper surface and a highly curved lower surface. The seating arrangement for configuration 1B is similar to 2A, i.e. a two-four arrangement.

D. Heat Shield Design

The following portions will break down the heat shield design into three sections: 1. Stagnation regions (which includes nose cap, leading edges and tail fins), 2. Lower surfaces, and 3. Upper surfaces.

From a review of the Apollo study which investigated a large number of thermal protection systems, it was decided that for fabrication simplicity, reliability and overall weight considerations, an ablation type heat shield design offers the best practical solution to the heating problem for the Multi-Mission Re-entry Vehicle in areas of high heating. An ablation design was utilized on the nose cap, leading edges, bottom surfaces and fins, while a radiation type heat shield was used on the cooler top surface.

Although the Multi-Mission Re-entry Vehicle is a manned spacecraft, the analysis in this report did not strive to limit the inside temperatures to living condition (i.e. approximately 70°F). Instead, the boundary for heating was the allowable temperatures of the materials used in the heat shield design. It is presently planned to insulate the cabin separately with a low density, high performance insulation material, the selection to be made in a continuing study.

1.0 Stagnation Regions

1.1 Nose Cap

The heat input to the nose cap is composed of two parts, the convective heat input and the equilibrium gas cap radiation input.

The convective heating rate at the spherical stagnation point was calculated by use of an existing IBM 7090 digital computer program (Reference 4) containing analysis equations from Goldstein (Reference 5) and utilizing the reference enthalpy method of Eckert (Reference 6). The convective heating stagnation heat flux on the 20-inch diameter nose cap of the Multi-Mission Vehicle is shown in Figure 6. The heat input by hot gas cap radiation is shown in Figure 7. A comparison of the two indicates that the radiation heat flux to the nose cap is a small portion of the total input, amounting to approximately 4% of the total heat input at the time of peak convective heating. The method used to compute the gas cap radiation was that of Kivel (Reference 2) and appears to give smaller values than the radiation fluxes calculated by Li-Geiger (Reference 7) methods.

From previous experience it was decided that for a low weight, high performance heat shield the construction would consist of sandwich layers of ablator, insulation and hot structure. Since the insulation and structure allowable temperatures would dictate the wall thickness and consequently the weight, high temperature Min-K 2000 and stainless steel honeycomb were selected.

The allowable temperatures of Min-K 2000 and stainless steel honeycomb are 2460°R and 1460°R respectively.

For the ablation type shield it can be seen that the ablation temperature and total heat input are directly related. For a heat flux greater than 10,000 Btu/ft^2 the use of a low ablation temperature material such as Avcoat 19 is not desirable; therefore, for a large heat input of over 20,000 Btu/ft^2 such as received at the stagnation regions from the lifting undershoot and drag overshoot trajectories for the Multi-Mission Vehicle, a high ablation temperature material such as Avcoat X-5026 or Avcoat X-5035 is desired. Whereas Avcoat X-5035 has a lower heat of ablation than Avcoat X-5026, it is approximately half as dense and analysis reveals that a definite weight saving was provided by the selection of this material.

The ablation temperature and effective heat of ablation of Avcoat X-5035 used in all the analyses was 5460°R and 8900 Btu/lb. respectively. Due to a lack of information of the effect that changes between the stagnation and wall enthalpy have on the effective heat of ablation, the Avcoat X-5035 was assumed to have a constant 8900 Btu/lb. heat of ablation throughout flight. Because Avcoat X-5035 has a high ablation temperature the effect of enthalpy changes is not as significant as with a low ablation temperature material; however, the interior skin temperatures predicted may be lower than calculated when the effective heat of ablation is used as a variable with enthalpy.

Figure 8 shows the temperature-time histories for various locations in the wall for the initial portion only of the drag overshoot trajectory. It can be seen from Figure 8 that the allowable temperatures of Min-K 2000 and stainless steel honeycomb have already been approached or reached, yet at this time of flight (352 seconds out of 4000 seconds) approximately 20% of the total integrated heat input has been applied to the wall. It therefore can be concluded that the heat shield wall in Figure 8 must be increased in thickness, and from a knowledge of the heat fluxes, configurations and heat shield materials a conservative design was selected for this preliminary study and is shown in Table 1.

1.1 Wing Leading Edge

The analytical technique used for the leading edge heating was the same as for the nose cap (Section D, 1.1) except to account for the leading edge yaw-angle to the airstream. This relationship was taken from Reference 8, based on experimental data showing the influence of yaw on average heat transfer rates to cylinders in high Mach number flow.

The Multi-Mission Re-entry Vehicle flies at a 60 degree angle of attack, the yaw relationship is not simply based on the geometric sweep angle (Figure 4, 5), but a combination of this angle with the angle of attack. This included angle was found to be approximately 60 degrees using both vector analyses and descriptive geometry. The yaw-angle therefore was 30 degrees and when used with Reference 8 results in heat rates which are 80 percent of the unyawed heating rates.

The heat input to the 12.5-inch diameter wing leading edge was again composed of two parts, the convective heat input and the equilibrium gas cap radiation input. The equilibrium gas cap radiation input was assumed to be the same as that for the nose cap and is shown in Figure 7. The temperature-time histories of various locations in a preliminary heat shield design for the heat limiting drag overshoot trajectory are shown in Figure 9. While Figure 9 represents only approximately 20% of the total integration heat flux to the wall, it can be seen that the Min-K and stainless steel allowable temperatures have already been reached. Consequently, based on a knowledge of the heating rate, heat shield materials and configuration, a conservative design was selected and is shown in Table 1.

1.3 Tail Fin Surfaces

Although the tail fins would normally be exposed to high heat fluxes during flight at low angle of attack, the Multi-Mission Re-entry Vehicle initially re-enters at a 60-degree angle of attack; and hence, when the angle of attack and tail fin sweep angles are combined it is expected that the heating on the fins will be considerably below that of stagnation heating. For this preliminary design an analysis was not performed on the tail fins and therefore, the optimum skin thickness is not known. However, a conservative design identical to the leading edge heat shield and bottom surface walls, shown in Table 1, was selected and used in the weight analysis.

2.0 Lower Surface

Bottom surface flow patterns for flat delta wings having a 70 degree sweep, a blunted nose and blunted leading edges were obtained from NASA data (Reference 9) and are shown in Figure 10 for a 60 degree angle of attack. Although the lower surface of the Multi-Mission Vehicle is not perfectly flat (Figures 4 and 5), it has the same sweep angle and will fly at 60 degrees angle of attack during the initial re-entry phase, therefore, the flow pattern on its lower surface will be very similar to that shown and should not alter centerline heating appreciably. An explanation of the flow pattern shown in Figure 10 is that at high angles of attack, the pressure distribution from the centerline outward to the leading edge exhibits a falling pressure which causes the boundary layer to diverge.

Aerodynamic heating calculations on the lower surface centerline were performed as indicated in Reference 9. A point on the center at a distance of 3 nose diameters from the stagnation point was selected as representative. Data obtained from Reference 9 were extrapolated for a delta wing at 60° angle of attack and the heating, which is thought to be slightly conservative, was determined at the location noted earlier. The severity of the entry heat flux (Figure 11) posed the problem of adequate protection of the basic vehicle structure. Two alternatives to the design were considered, use of existing ablation materials having a relatively high ablation temperature (and low density) and materials having a low ablation temperature (and high density). It was found that the thickness of low ablation temperature, high density material required would result in a greater initial weight than the high ablation temperature materials because of the need for the ablayor to provide the necessary temperature drop to the Avcoat ablator - Min-K interface. Radiation systems are in general restricted to flight regimes having low rates of aerodynamic heating, due to service temperature limits on the skin and insulator, hence, no attempt was made to study refractory metal systems of this type.

After selecting a low density, low conductivity ablator for the vehicle outer surface, it remained to narrow the selection of the trajectory. The design of the heat protection system would utilize the trajectory yielding the greatest total heat load in order to prevent structural temperatures from exceeding maximum allowables. The drag overshoot trajectory whiwn in Figure 1 was used as the reference. Figure 12 gives some isochronal temperature gradients through Avcoat 5035 ablator and an insulator designated as Min-K 2000. Although the Min-K 2000 is not truly a high strength insulator, it may be sufficiently strong for lifting re-entry vehicles design. Min-K 2000 is one of the first materials developed from consideration of the fundamental principles of heat transfer in fibrous insulators, and there fore is very efficient.

The heat flux history shown in Figure 11 and the resulting temperatures in Figure 12 seem to indicate an adequate design, in fact, a margin of overdesign appears to exist when the temperature history is plotted for the Avcoat 5035 Min-K 2000 interface (Figure 13). However, the drag overshoot trajectory may be expected to have flight times of durations lasting to 4000 seconds, at about a 17° angle of attack. In this case, the average heat input to the surface may approximate 20% of the peak rate shown in Figure 11 and the heat input must be accounted for. Experience has shown that isochronal peaks such as those in Figure 12 will shift to distances further removed from the outer surface so that the maximum allowable temperature of 2460°R for the Min-K 2000 would be exceeded beyond 350 seconds of flight. Since no heat flux data were obtained for the entry portion of flight other than a 60° angle of attack (first 350 seconds), estimates were made of the thickness of materials required for extended flight times when the entry maneuvers would change. Overall thicknesses are given in Table 1 showing a conservative design of 0.75" Avcoat 5035, 1.0" Min-K 2000, and 0.50" stainless steel honeycomb with 0.01" stainless steel facings. The local weight of this composite is 5.0 lbs/ft^2.

3.0 Upper Surface

Because the Multi-Mission Vehicle flies at a large angle of attack to maintain lift during re-entry, the airflow over the upper surface remains separated. Aerodynamic heating of these surfaces was assumed to be .7 of attached turbulent flow based upon correlations presented in Reference 10. The convective heat flux calculated at 1 foot and 10 feet positions on the upper surface are shown in Figure 14. For these calculations the initial phase of the drag overshoot trajectory and the coast phase of the trajectory were faired together at a velocity of 24,400. This results in a total trajectory time of 3200 seconds, approximately 800 seconds shorter than the total time used for the stagnation region and lower surface calculations.

3.1 Skin Area

The temperatures of the upper surface wall were calculated for three positions, 1 foot, 5 feet and 10 feet aft of the stagnation line. A wall configuration employing radiation heat shield design principals was chosen for analysis since temperatures in the order of 2000°R to 2500°R are typical of separated flow heating during re-entry. The particular design studied has ADL-17 powder encapsulated in Inconel X to insulate the underlying vehicle structure (Reference 11). The outer surface of the Inconel X container acts as the radiating heat shield and will operate satisfactorily at temperatures up to 2460°R (Reference 12).

Figure 15 shows the temperatures calculated for both the outer and inner surfaces. Because the underlying stainless steel structure is temperature limited at 1460°R, it is apparent that the thickness of the ADL-17 power may be reduced. This could result in a weight saving of approximately .2 to .3 pounds per square foot. A half-section, plan view of the re-entry vehicle is also shown with isotherms at the three distances studied measured aft from the leading edge in the direction of the vehicle axis. However, high angles of attack may cause the flow to be more normal to the leading edge.

3.2 Viewing Port

Vycor glass was studied for the pilot viewing port located near the center of the vehicle. This type of glass has good thermal conductivity thereby minimizing temperature induced strains. Temperatures calculated for a .75 inch thick viewing port are shown in Figure 15. Since these temperatures are higher than those suitable for cabin inner wall temperature, an inner layer of heat resisting glass should be provided preferably with an air gap between it and the Vycor.

E. Weight Analysis

The total vehicle heat shield weight was based on the summation of the weight of the heat shield at six vehicle locations: (1) nose cap, (2) wing leading edges, (3) Tail fins, (4) bottom surface, (5) Upper surface, and (6) viewing port. The total vehicle heat shield weight was calculated by multiplying the weight per unit area of a particular heat shield design times the total area of that location. The local and total weight breakdown is shown in Table 2.

CONCLUSIONS

Due to the preliminary nature of this study some assumptions were necessary for the completion of the heat shield and weight analysis. To briefly summarize the assumptions: (1) Considered all convective heating as continuum flow (2) Considered the effective heat of ablation of the Avcoat X-5035 material as constant throughout flight, (3) Considered the combination of the initial and coast trajectories as a step-function, (4) assumed coast phase was approximately 80% of integrated heat flux, (5) assumed aerodynamic heating on top surface to be 0.7 of attached turbulent flow, (6) assumed radiation heating from gas cap as equilibrium heating throughout flight, and finally (7) the bottom surface was treated as a flat surface rather than curved. It might be stated that the degree to which each assumption effects the total heating is not accurately predictable; however, it is felt that none of the assumptions singularly produce any large errors in the analysis and furthermore somewhat offset each other. To support this latter statement it may be noted by study that the first four assumptions appear to have the effect of increasing the heat input while the last two assumptions appear to lower the heat input to the vehicle. Nevertheless, it is felt that the included vehicle heat shield design is conservative. although preliminary.

REFERENCES

1. Brunner, M. J., "Aerodynamic and Radiant Heat Input to Space Vehicles Which Re-Enter at Satellite and Escape Velocity," ARS Journal, Vol. 31, No. 8, August 1961

2. Kivel, Bennett, "Radiation From Hot Air and Stagnation Heating," AVCO-Everett Research Report 79, October 1959

3. Camm, J. C., Kivel, B., Taylor, R. L. and Teare, D., "Absolute Intensity of Non-Equilibrium Radiation in Air and Stagnation Heating at High Altitudes," AVCO Research Laboratory Report 93, December 1959

4. Cohen, A., "A Stable Numerical Solution of Transient Heat Conduction Problems," General Dynamics/Astronautics Report AE60-0744, 8 Sept. 1960

5. Goldstein, S., "Mod. Developments in Fluid Dynamics," Oxford Univ. Press, Oxford, England, 1943, Vol. 2, pg 683

6. Eckert, E.R.G., "Survey on Heat Transfer at High Speeds," Wright Air Development Center, TR 54-70, 1954

7. Li, Ting-Yi, Geiger, R. E., "Stagnation Point of a Blunt Body in Hypersonic Flight Speeds," Jet Propulsion, April 1958, pg. 259

8. Cunningham, B. E., Kraus, Samuel, "Experimental Investigation of the Effect of Yaw on Rates of Heat Transfer to Transverse Circular Cylinders in a 6500 Foot-Per-Second Hypersonic Air Stream," Ames Aeronautical Laboratory, NACA-RM-A58E19, August 26, 1958

9. Bertram, Mitchel, H., and Henderson, Jr., Arthur, "Recent Hypersonic Studies of Wings and Bodies," ARJ Journal, August, 1961

PRIVATE DATA

10. Stolarik, E., "Notes on Flow Regimes and Wake Heating of Re-entering Vehicles," 14 September 1961, GD/Astronautics ERR-AN-083

11. Wechsler, A., Arthur D. Little, Inc. "Advances in High-Temperature Thermal Protection Systems," AFOSR Conference on Aerodynamically Heated Structures, July 25-26, 1961, Cambridge, Mass.

12. Dickson, J., Bell Aerosystem Company, "Thermal Protection with a Temperature Capability to 2500°F for Cool Structures," AFOSR Conference on Aerodynamically Heated Structures, July 25-26, 1961 Cambridge, Mass.

MULTI - MISSION R/V
NOSE CAP, LEADING EDGE & BOTTOM SURFACE
HEAT SHIELD DESIGN PARAMETERS

LOCATION - DESIGN -	MATERIALS	DENSITY LBS/FT^3	THERMAL CONDUCTIVITY BTU/FT HR °R	SPECIFIC HEAT BTU/LB °R	WEIGHT LBS/FT^2
NOSE CAP 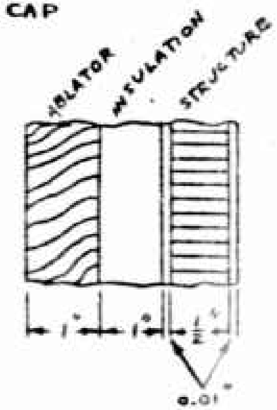	AVCOAT X 5035	36	0.06	0.35	3.00
	MIN-K 2000	20	0.0417	0.27	1.67
	STAINLESS STEEL FACINGS	490	10	0.13	0.82
	STAINLESS STEEL HONEYCOMB	6	0.11	0.13	0.25
					5.74
LEADING EDGES & BOTTOM SURFACE 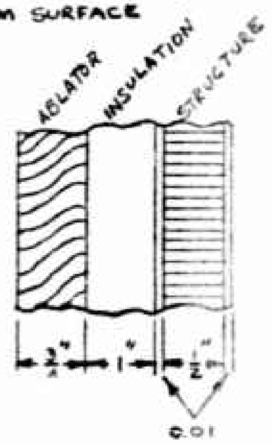	AVCOAT X 5035	36	0.06	0.35	2.25
	MIN - K 2000	20	0.0417	0.27	1.67
	STAINLESS STEEL FACINGS	490	10	0.13	0.82
	STAINLESS STEEL HONEYCOMB	6	0.11	0.13	0.25
					4.99

TABLE 1

PRIVATE DATA

MULTI-MISSION R/V

LOCAL & TOTAL HEAT SHIELD WEIGHT BREAKDOWN

LOCATION	WEIGHT - POUNDS CONF 2A	CONF. 1B	CONF. 2B	CONF. 3B
NOSE CAP	185	151	176	173
WING LEADING EDGES	156	0	314	204
TAIL FINS	823	623	807	814
BOTTOM SURFACE	1598	1568	1585	1627
UPPER SURFACE	771	753	805	810
VIEWING PORT	84	84	19	84
TOTAL HEAT SHIELD WEIGHT	3616	3179	3706	3712

TABLE 2

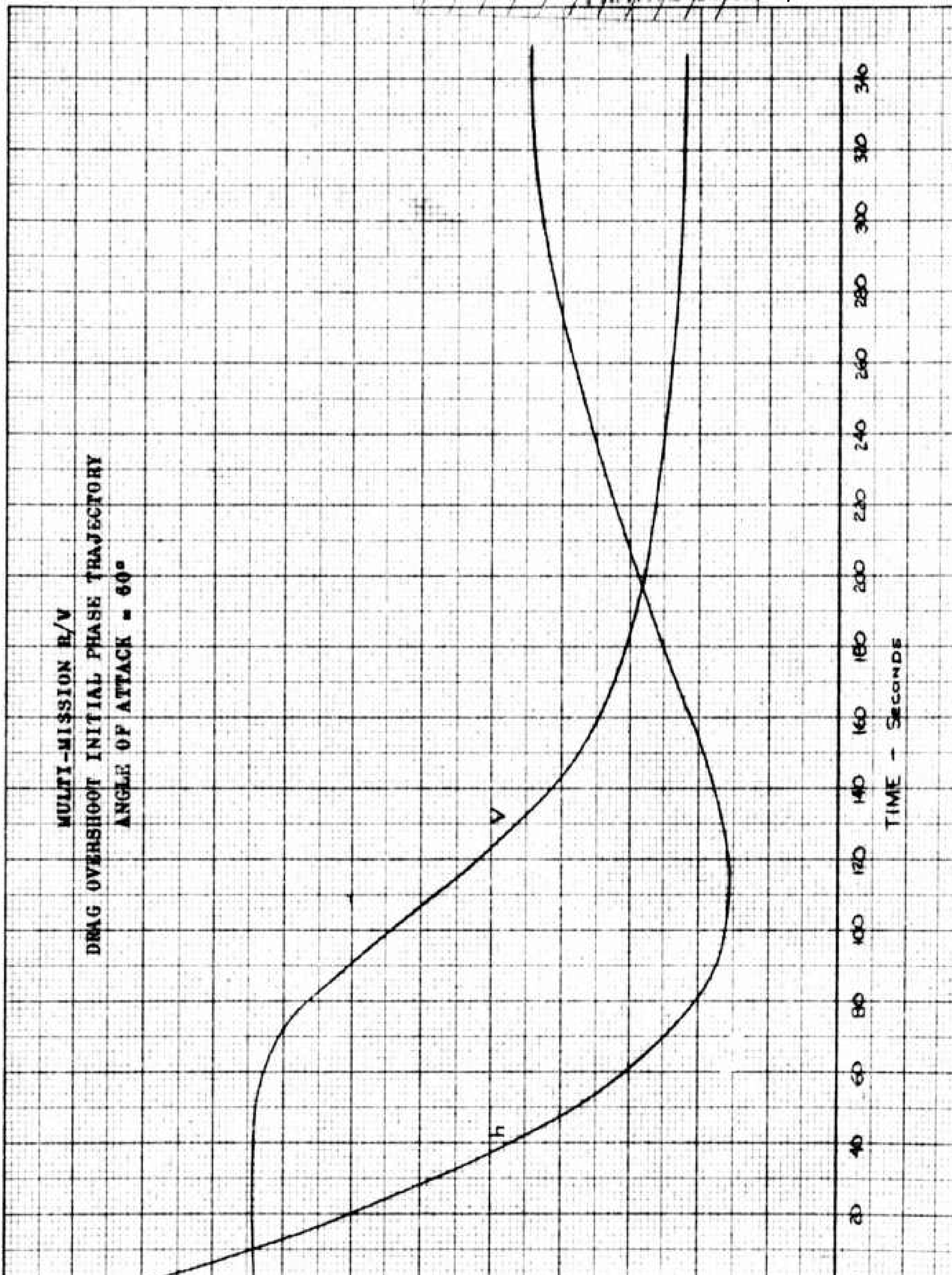
MULTI-MISSION R/V
DRAG OVERSHOOT INITIAL PHASE TRAJECTORY
ANGLE OF ATTACK = 60°
V
h
TIME - SECONDS
ALTITUDE, h - FEET x 10⁻⁴
VELOCITY, V - Ft/Sec x 10⁻³
0 20 40 60 80 100 120 140 160 180 200 220 240 260 280 300 320 340
40 38 36 34 32 30 28 26 24 22 20

FIGURE 1

PRIVATE DATA

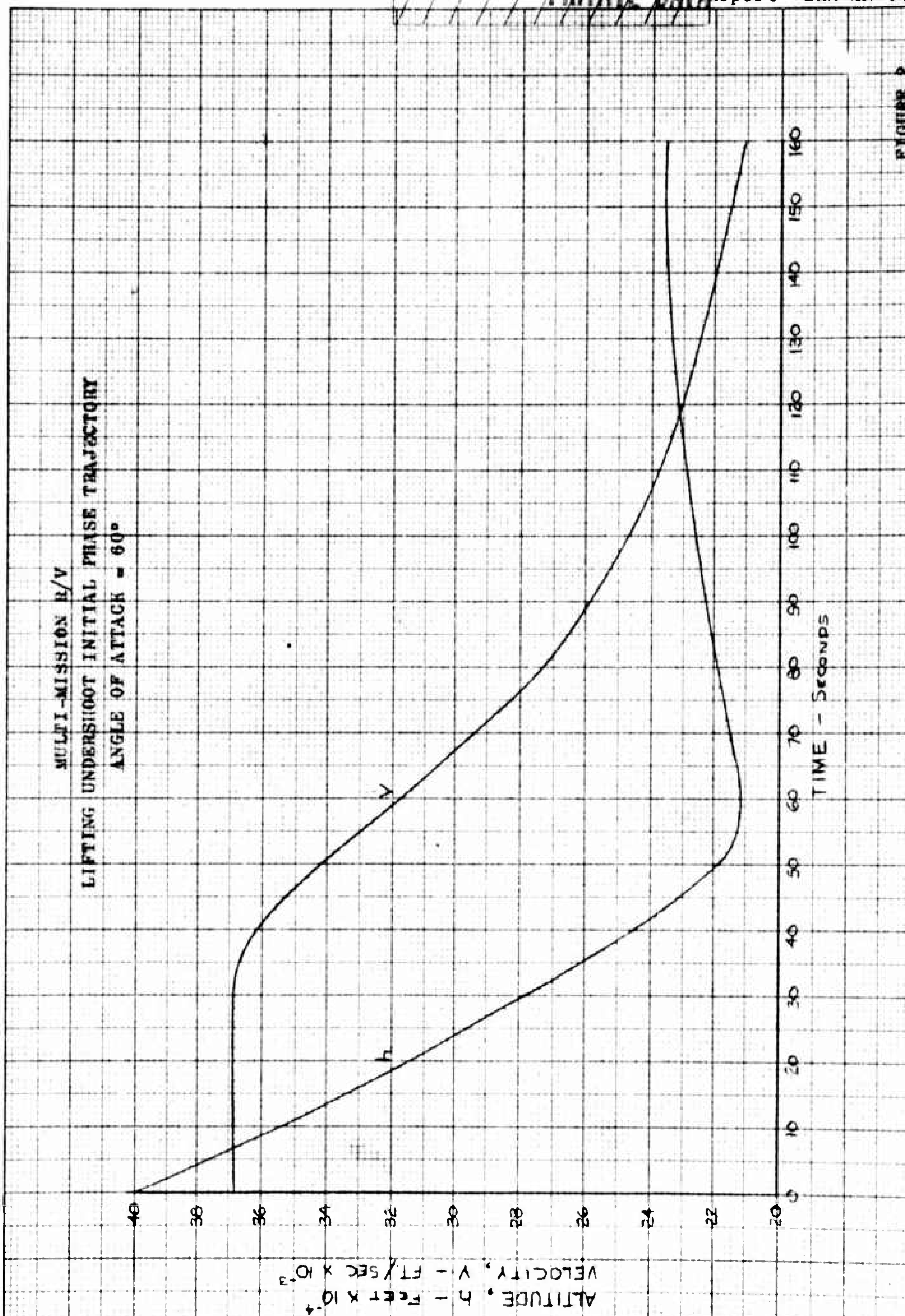

FIGURE 2

PRIVATE DATA

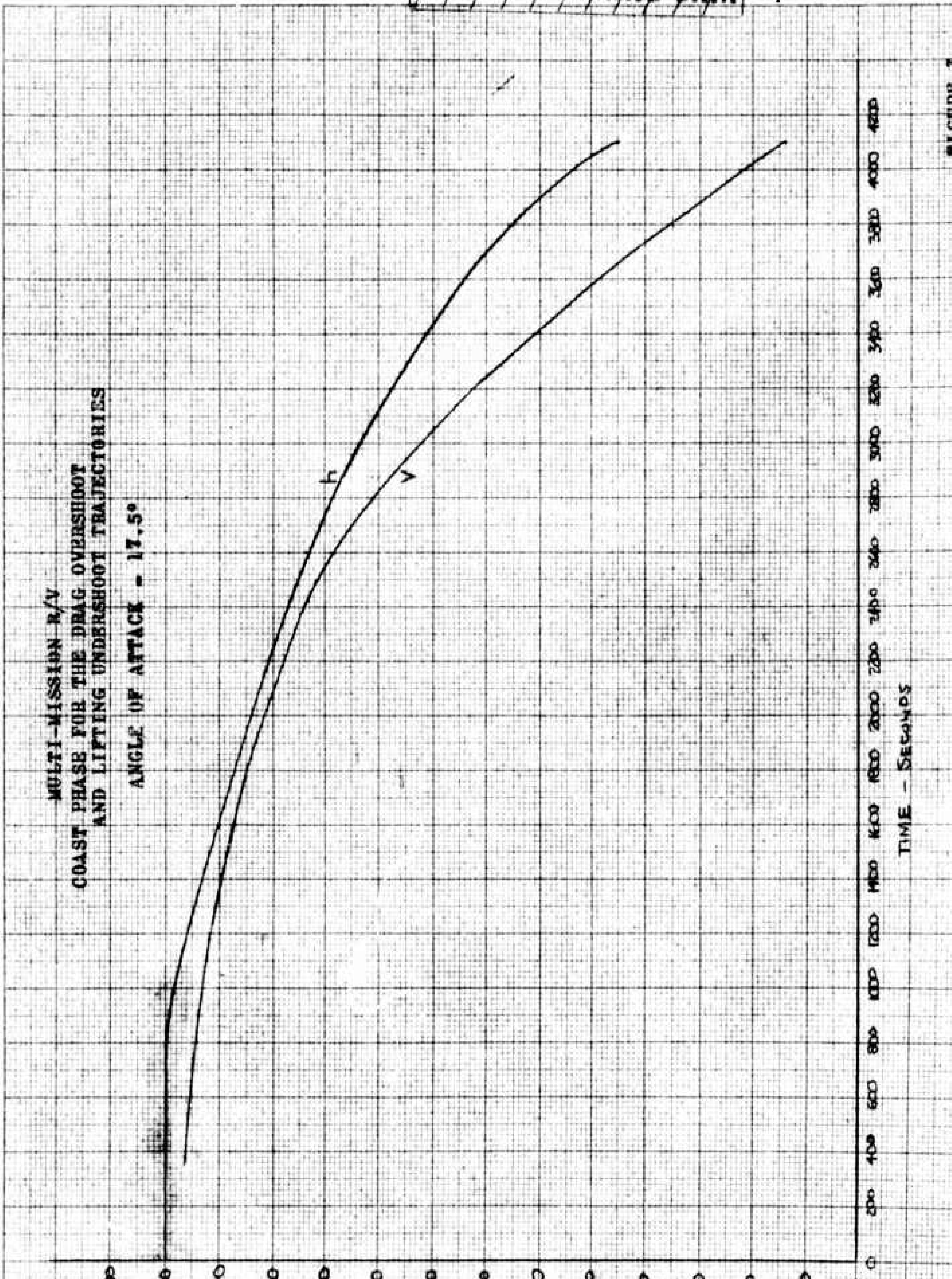
MULTI-MISSION R/V
COAST PHASE FOR THE DRAG OVERSHOOT
AND LIFTING UNDERSHOOT TRAJECTORIES
ANGLE OF ATTACK = 17.5°
h
V
TIME - SECONDS
ALTITUDE, h — FEET x 10^-3
VELOCITY, V — FT/SEC x 10^-2
0
200
400
600
800
1000
1200
1400
1600
1800
2000
2200
2400
2600
2800
3000
3200
3400
3600
3800
4000
4200
20
40
60
80
100
120
140
160
180
200
220
240
260
280

FIGURE 3

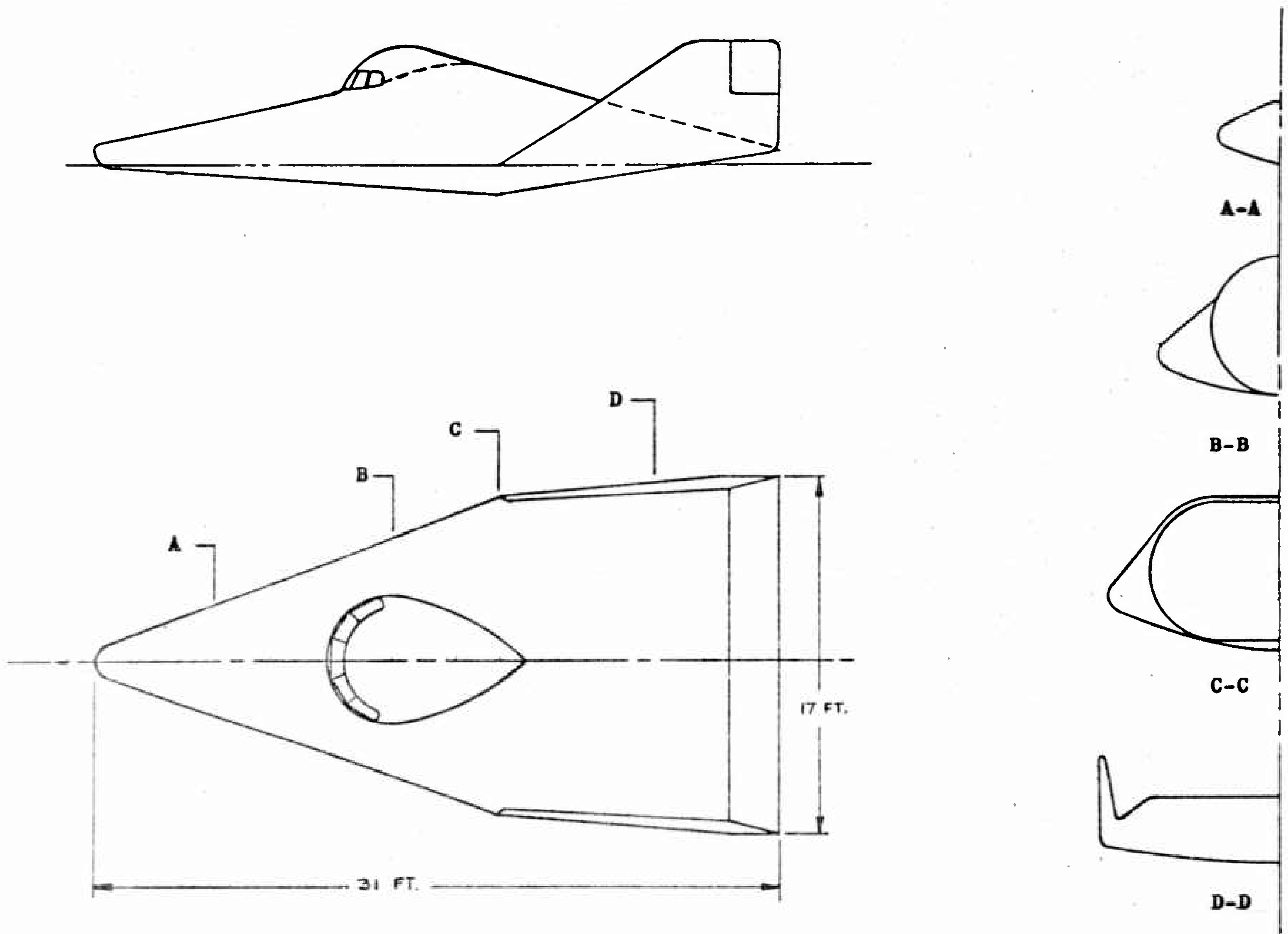

MULTI-MISSION 6-MAN
RE-ENTRY VEHICLE CONFIGURATION 2A

FIGURE 4

CGF 11/1/61

PRIVATE DATA

PRIVATE DATA

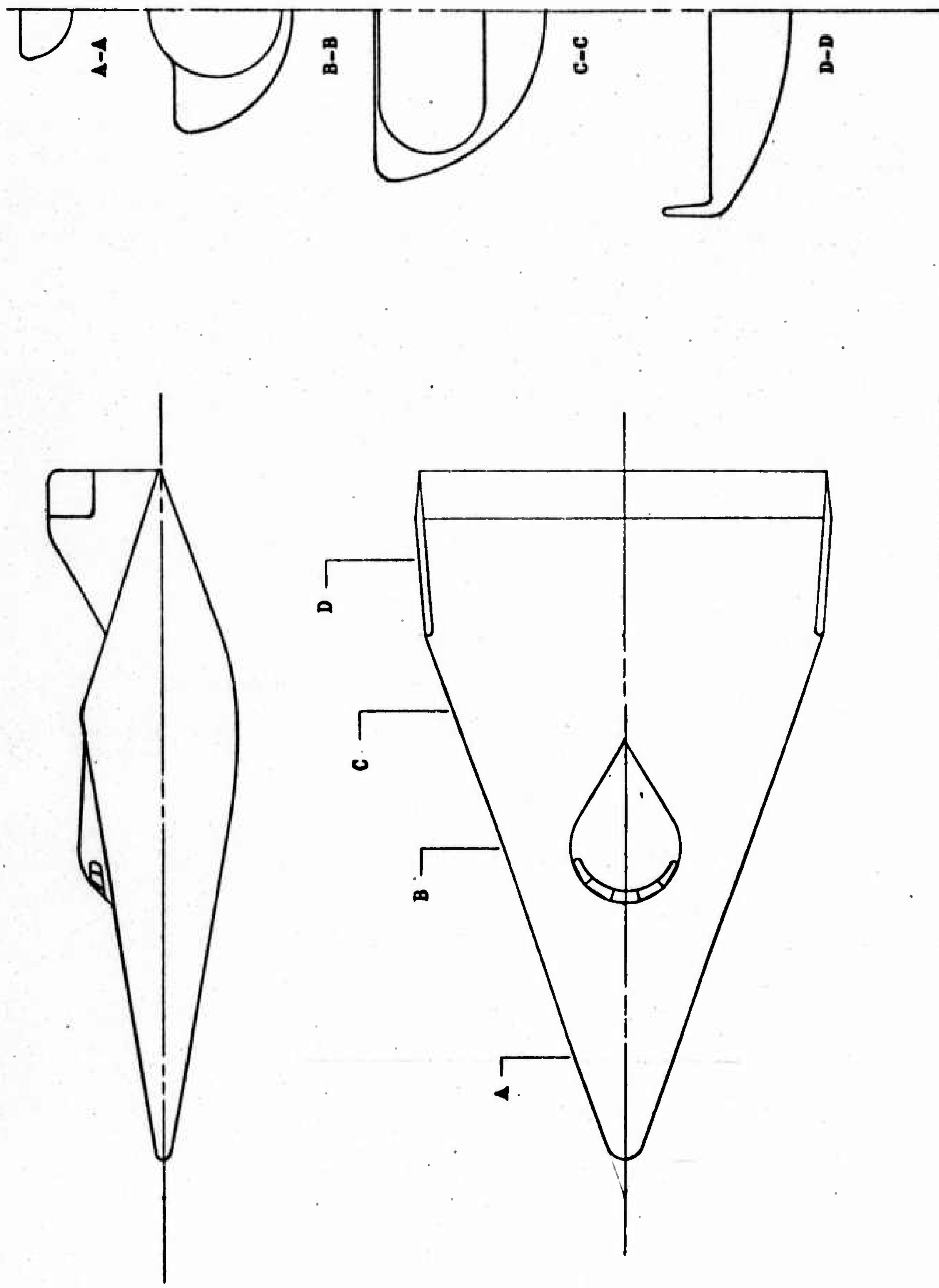

FIGURE 5

MULTI-MISSION 6-MAN
RE-ENTRY VEHICLE CONFIGURATION 1B

CGF 11/1/61

PRIVATE DATA

PRIVATE DATA

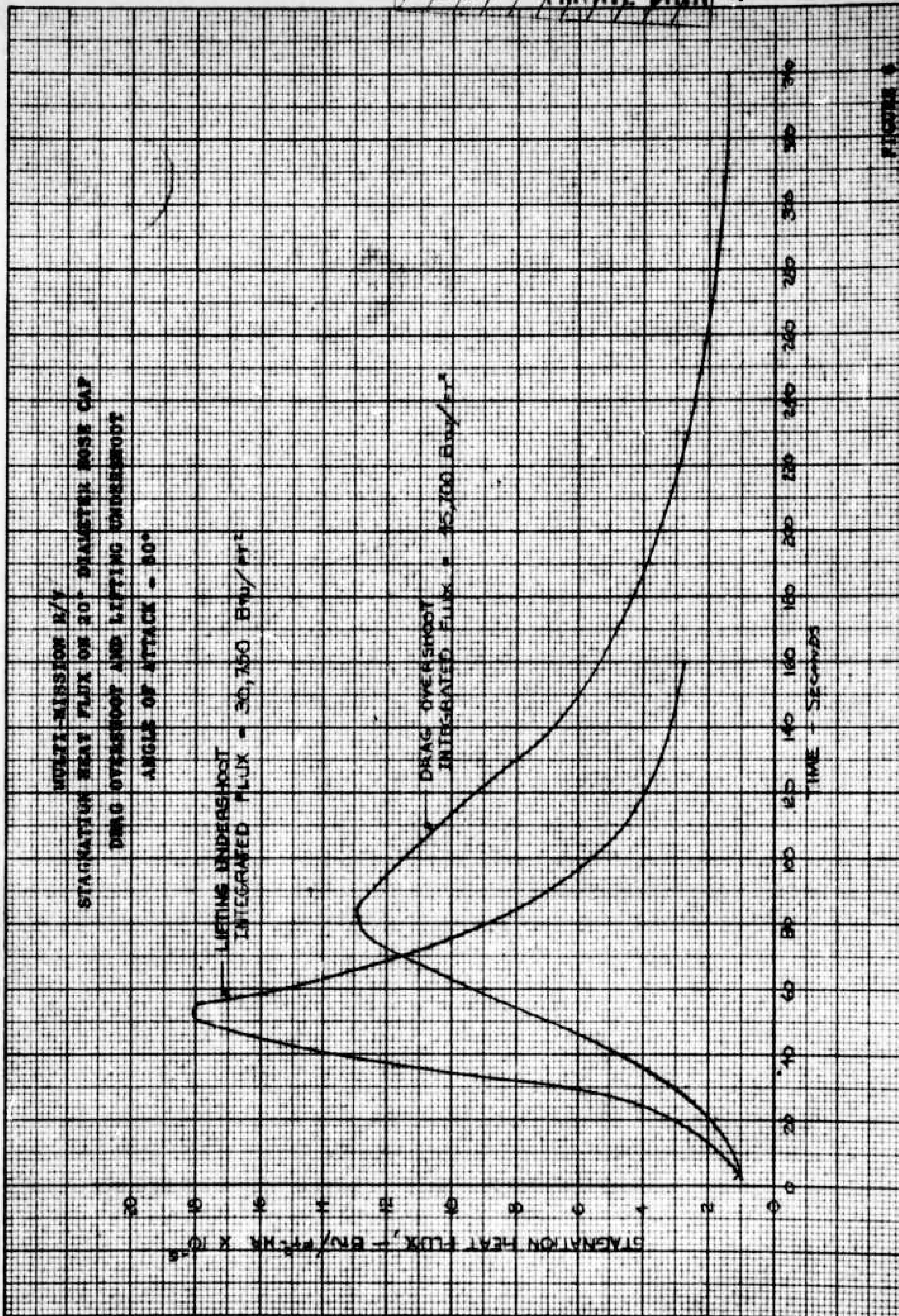

PRIVATE DATA

MULTI-MISSION R/V

HOT GAS GAP RADIATION*

DRAG OVERSHOOT ————

LIFTING UNDERSHOOT – – – – –

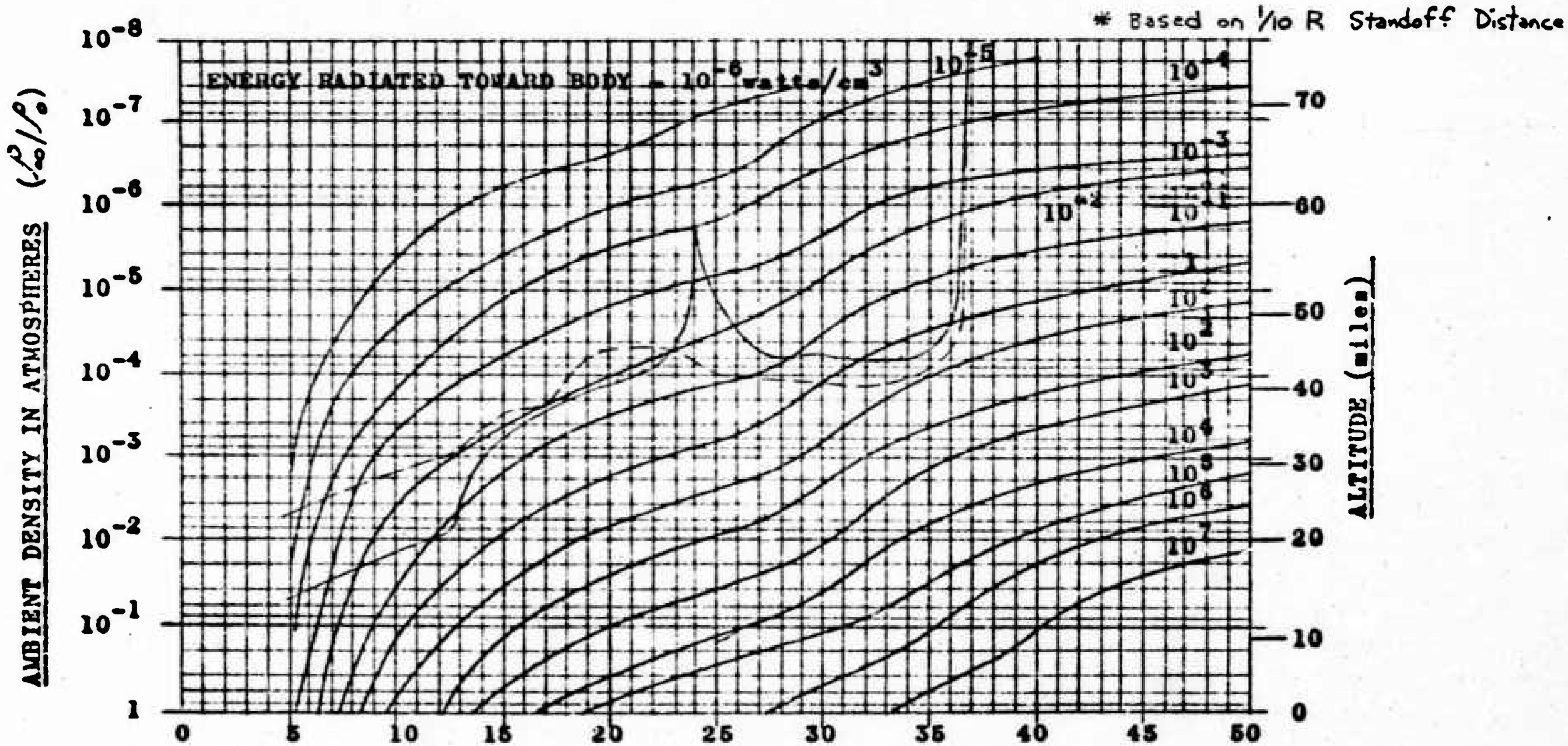

VELOCITY (kilofeet/sec)

One-half of the emitted radiation energy per unit volume from the stagnation region for full equilibrium as a function of ambient density and flight velocity.

FIGURE 7

FIGURE 7

PRIVATE DATA

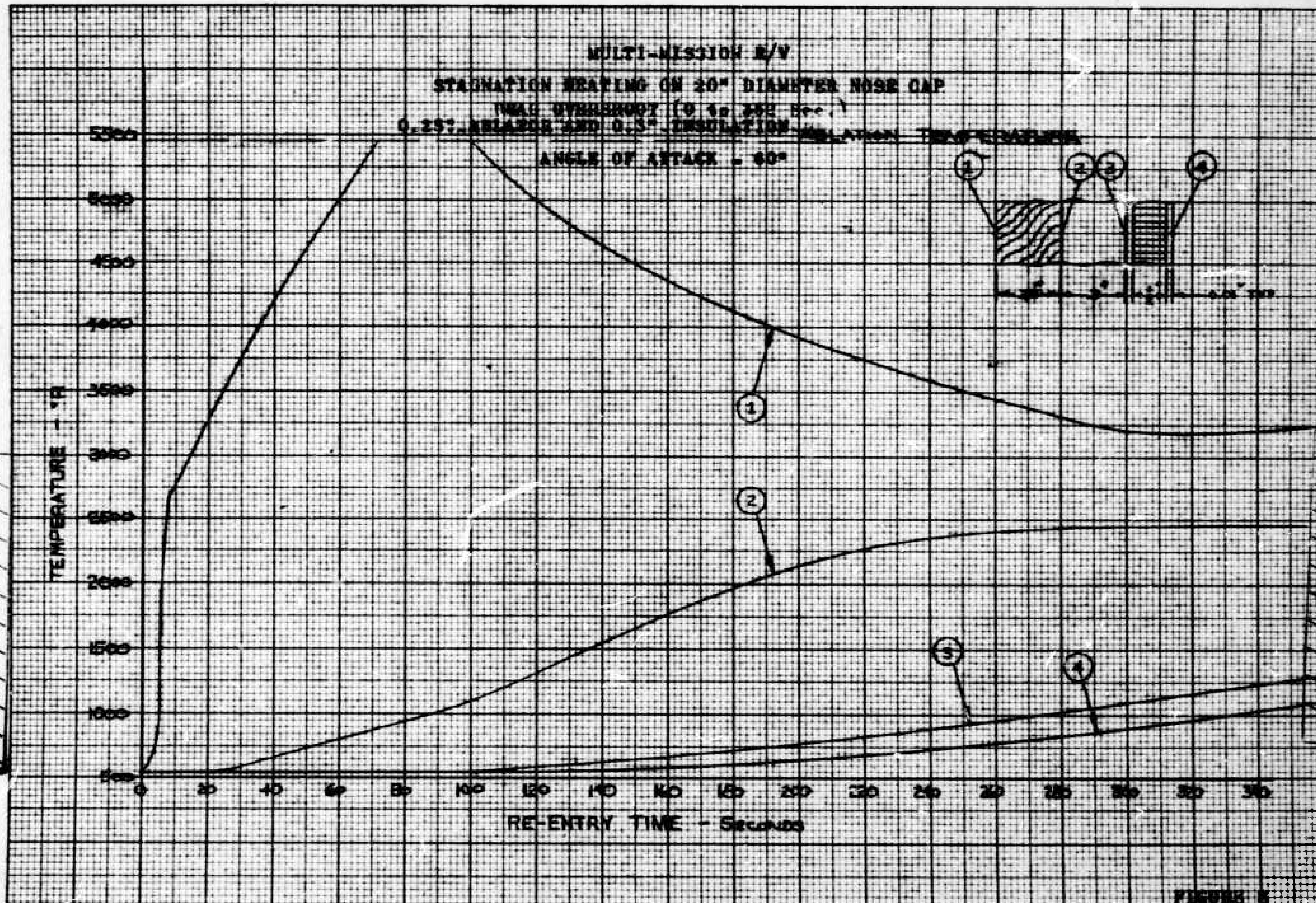

FIGURE 8

PRIVATE DATA

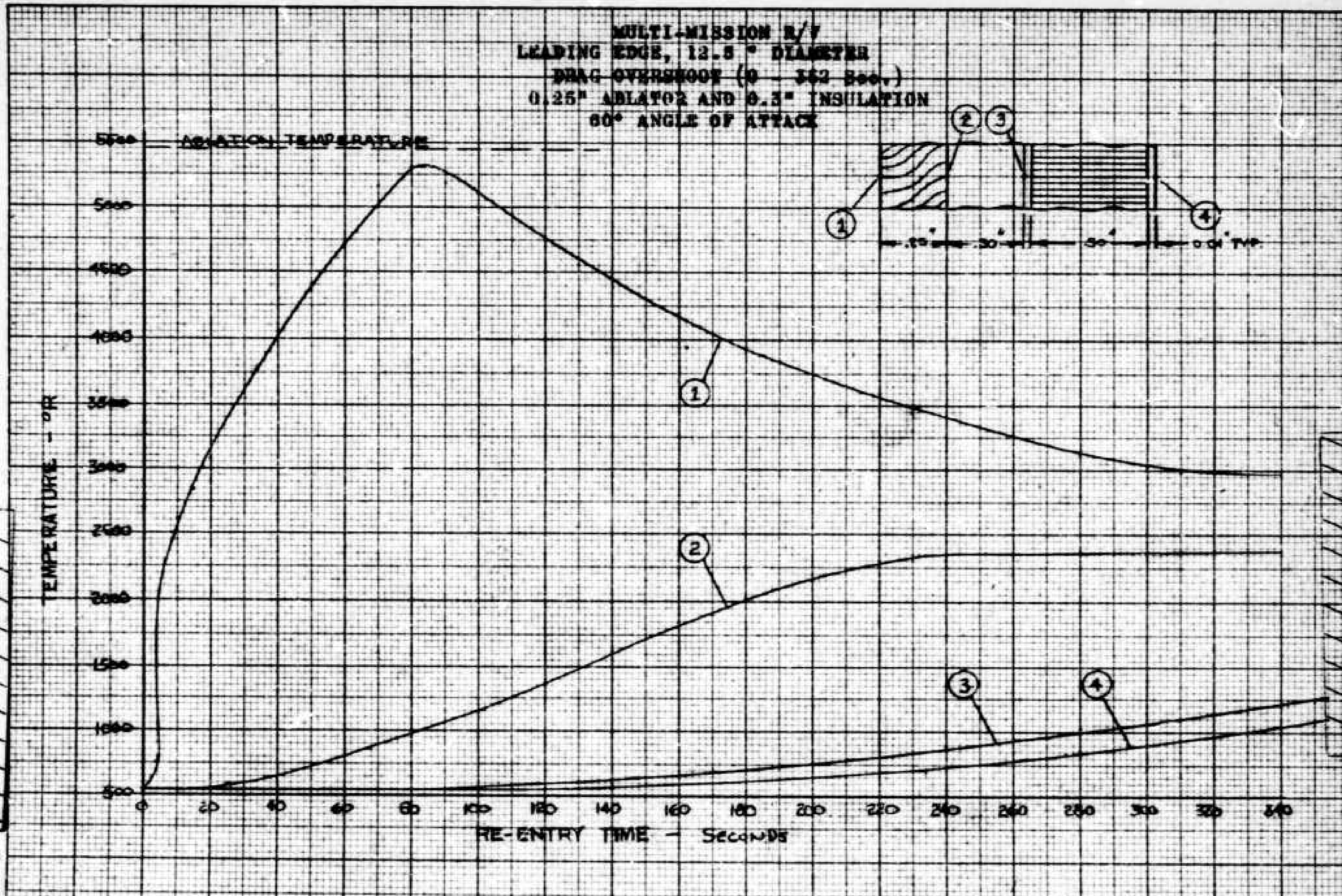

FIGURE 9

PRIVATE DATA

LOWER SURFACE HYPERSONIC FLOW
PATTERN ON A DELTA WING

SWEEP ANGLE = 70°
ANGLE OF ATTACK = 60°

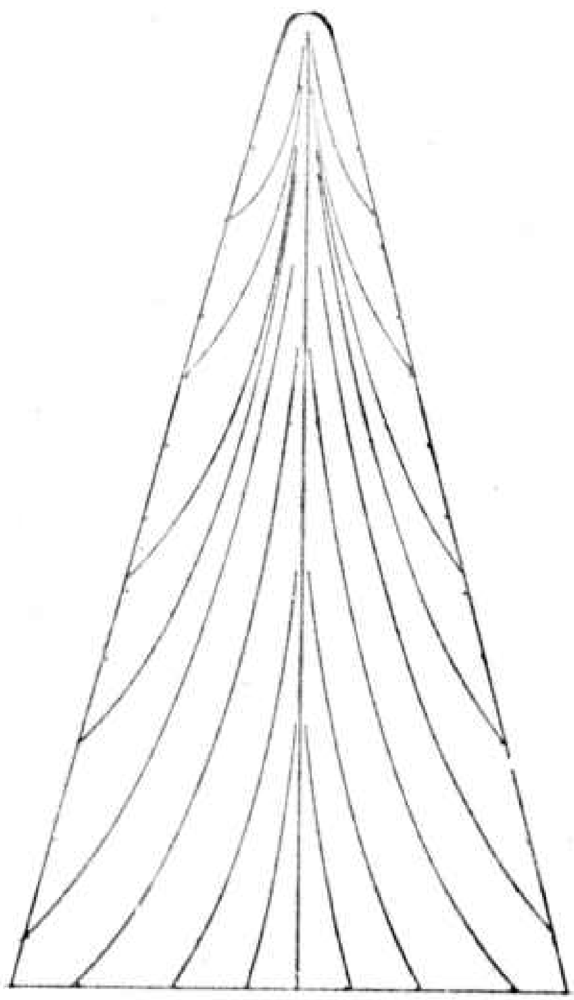

FIGURE 10

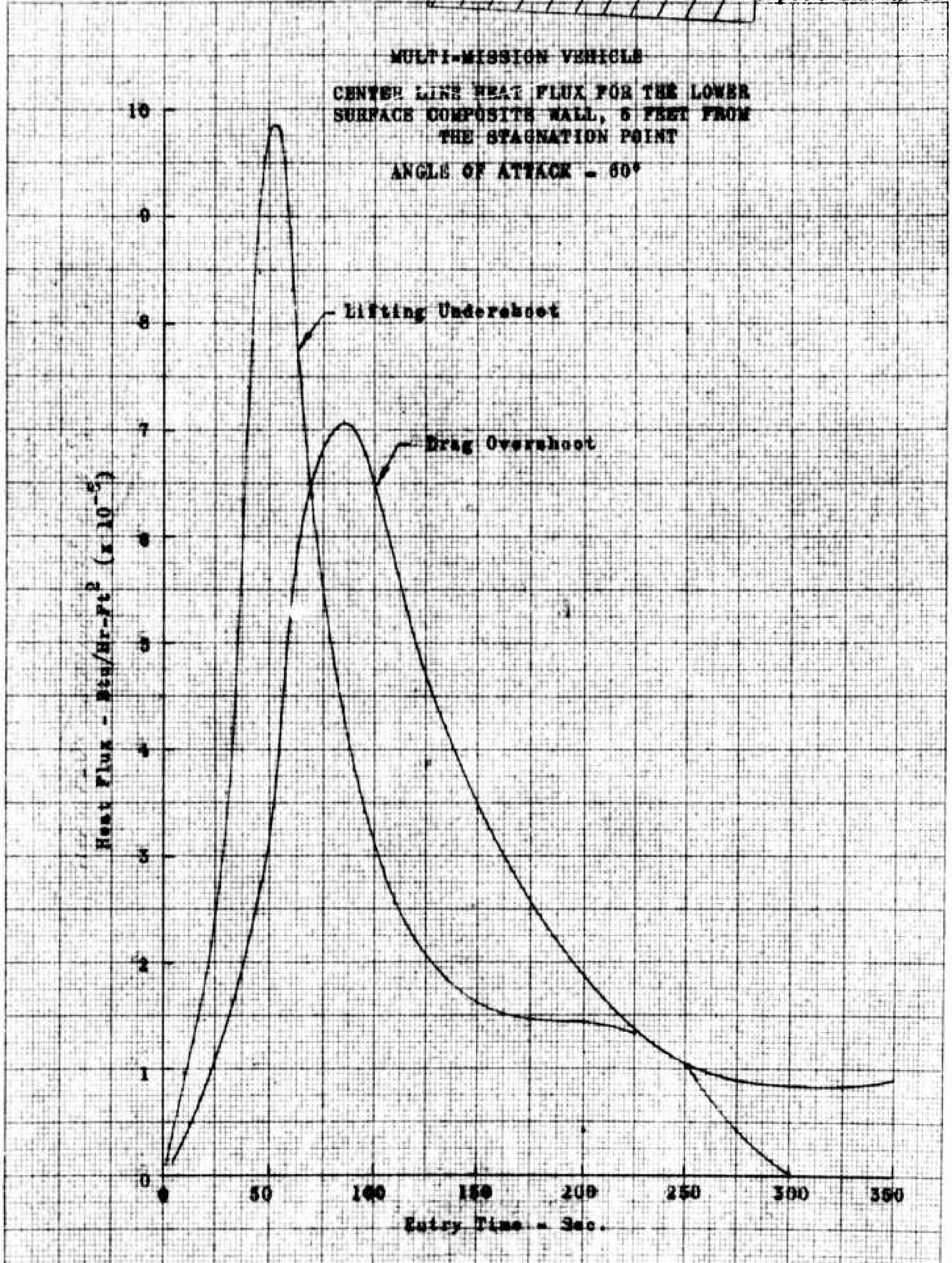
MULTI-MISSION VEHICLE
CENTER LINE HEAT FLUX FOR THE LOWER SURFACE COMPOSITE WALL, 5 FEET FROM THE STAGNATION POINT
ANGLE OF ATTACK - 60°
Lifting Undershoot
Drag Overshoot
Heat Flux - Btu/Hr-Ft^2 (x 10^{-5})
Entry Time - Sec.
0
1
2
3
4
5
6
7
8
9
10
50
100
150
200
250
300
350

FIGURE 11

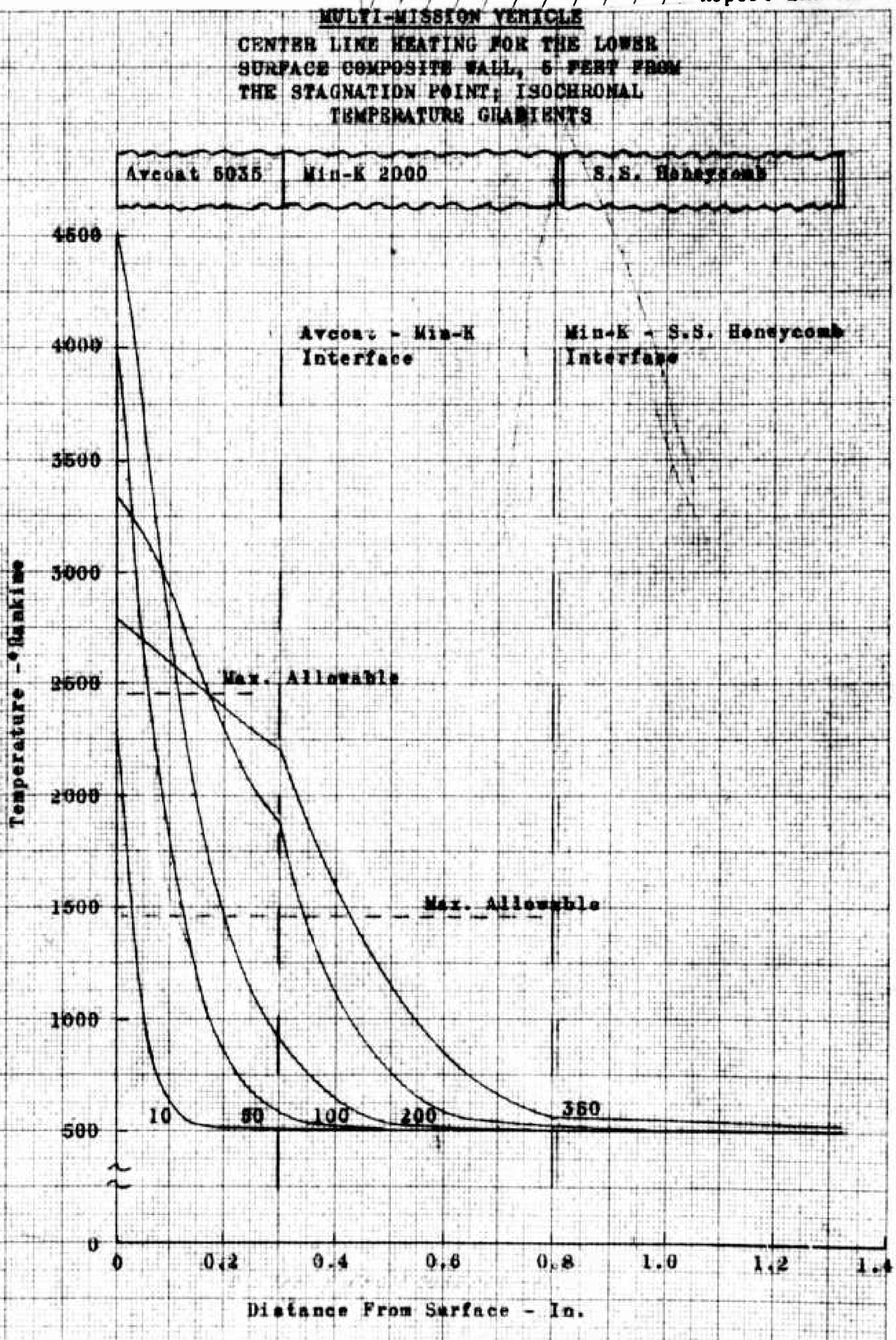
MULTI-MISSION VEHICLE
CENTER LINE HEATING FOR THE LOWER SURFACE COMPOSITE WALL, 5 FEET FROM THE STAGNATION POINT; ISOCHRONAL TEMPERATURE GRADIENTS
Avcoat 5035
Min-K 2000
S.S. Honeycomb
Avcoat - Min-K Interface
Min-K - S.S. Honeycomb Interface
Max. Allowable
Max. Allowable
Temperature - °Rankine
4500
4000
3500
3000
2500
2000
1500
1000
500
0
10
50
100
200
360
0
0.2
0.4
0.6
0.8
1.0
1.2
1.4
Distance From Surface - In.

FIGURE 12

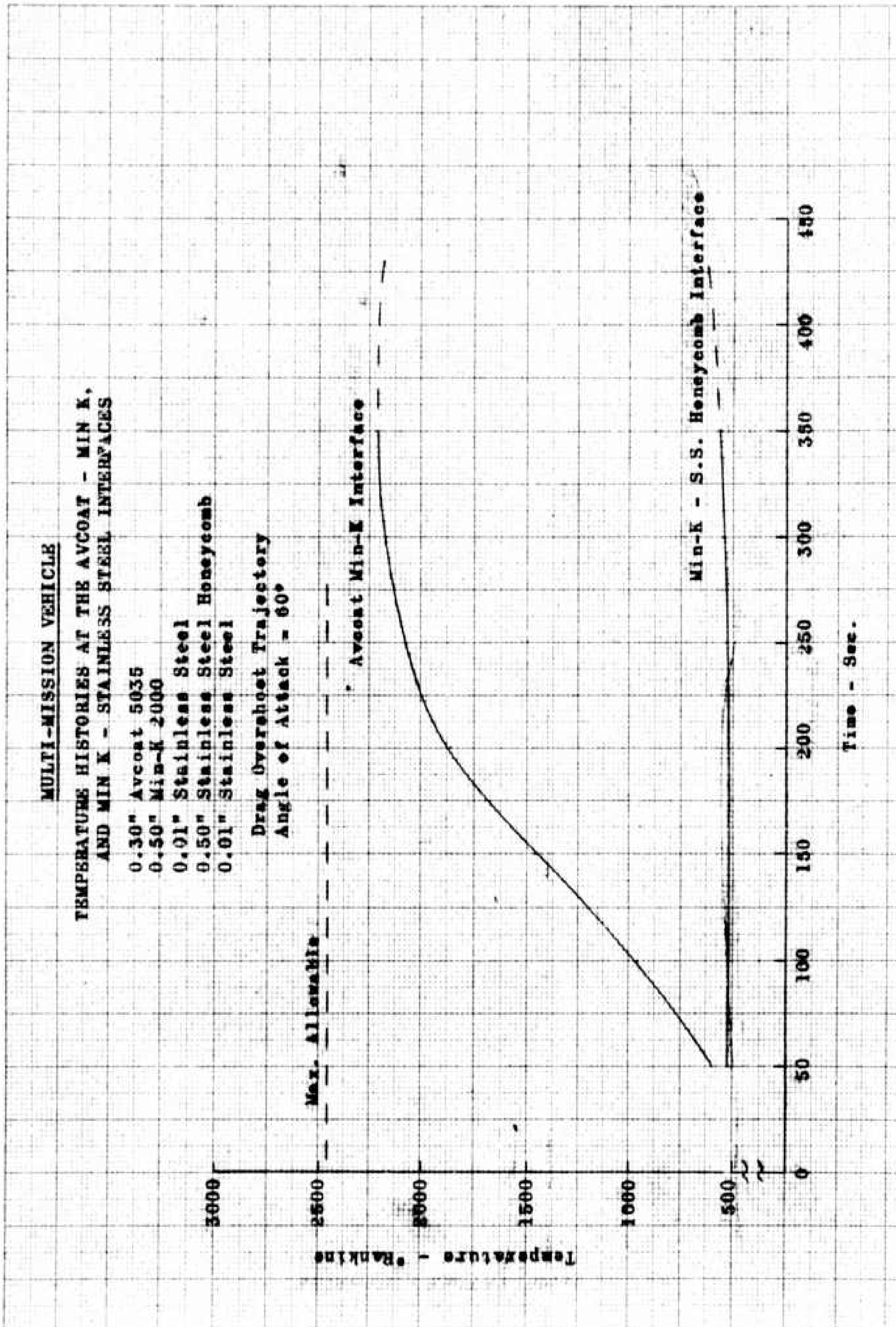
MULTI-MISSION VEHICLE
TEMPERATURE HISTORIES AT THE AVCOAT - MIN K, AND MIN K - STAINLESS STEEL INTERFACES
0.30" Avcoat 5035
0.50" Min-K 2000
0.01" Stainless Steel
0.50" Stainless Steel Honeycomb
0.01" Stainless Steel
Drag Overshoot Trajectory
Angle of Attack = 60°
Max. Allowable
Avcoat Min-K Interface
Min-K - S.S. Honeycomb Interface
Temperature - °Rankine
3000
2500
2000
1500
1000
500
0
50
100
150
200
250
300
350
400
450
Time - Sec.

FIGURE 13

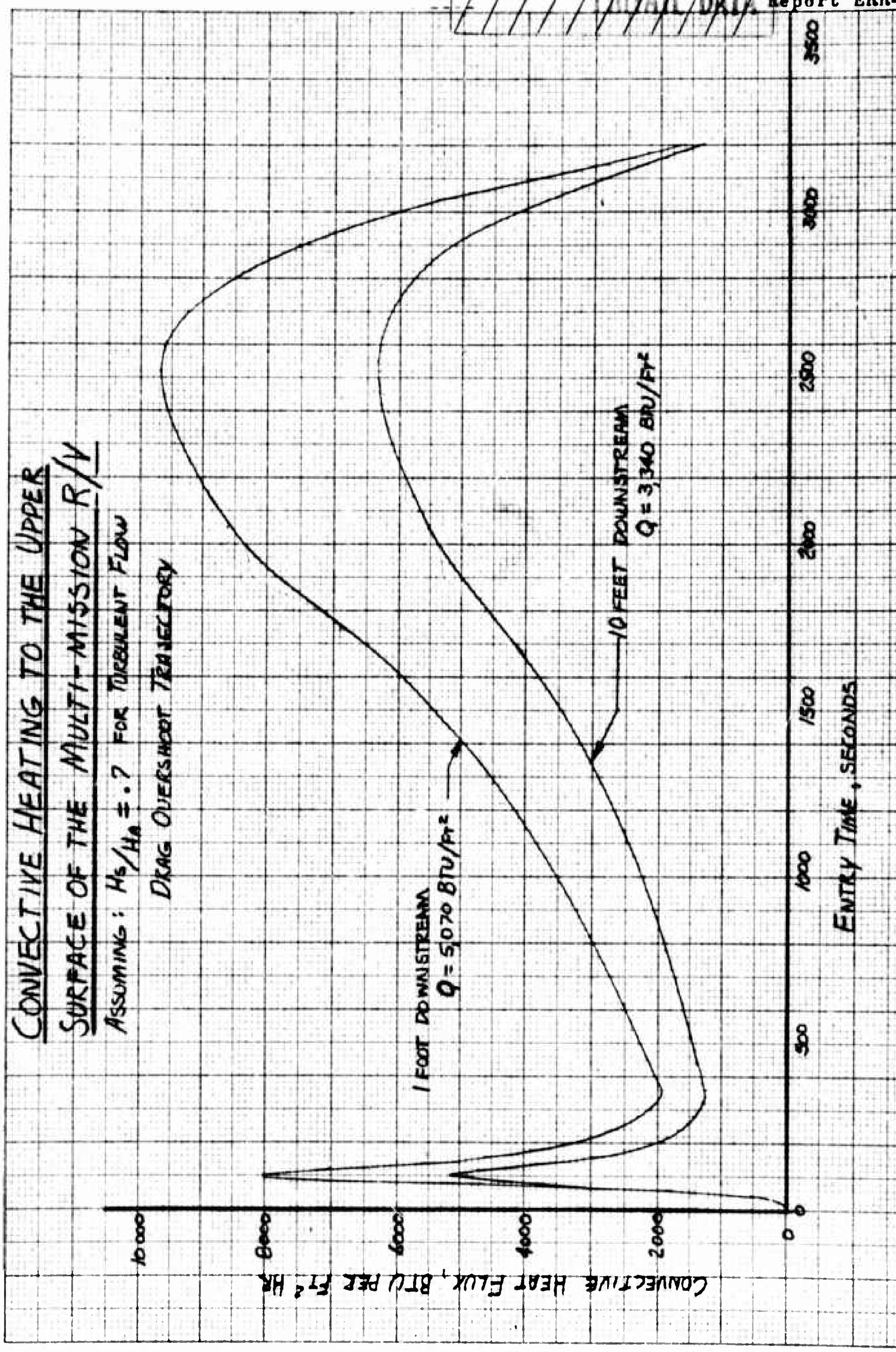
CONVECTIVE HEATING TO THE UPPER
SURFACE OF THE MULTI-MISSION R/V
ASSUMING: Hs/Ha = .7 FOR TURBULENT FLOW
DRAG OVERSHOOT TRAJECTORY
1 FOOT DOWNSTREAM
Q = 5,070 BTU/FT²
10 FEET DOWNSTREAM
Q = 3,340 BTU/FT²
0
500
1000
1500
2000
2500
3000
3500
ENTRY TIME, SECONDS
0
2000
4000
6000
8000
10000
CONVECTIVE HEAT FLUX, BTU PER FT² HR

FIGURE 14

PRIVATE DATA

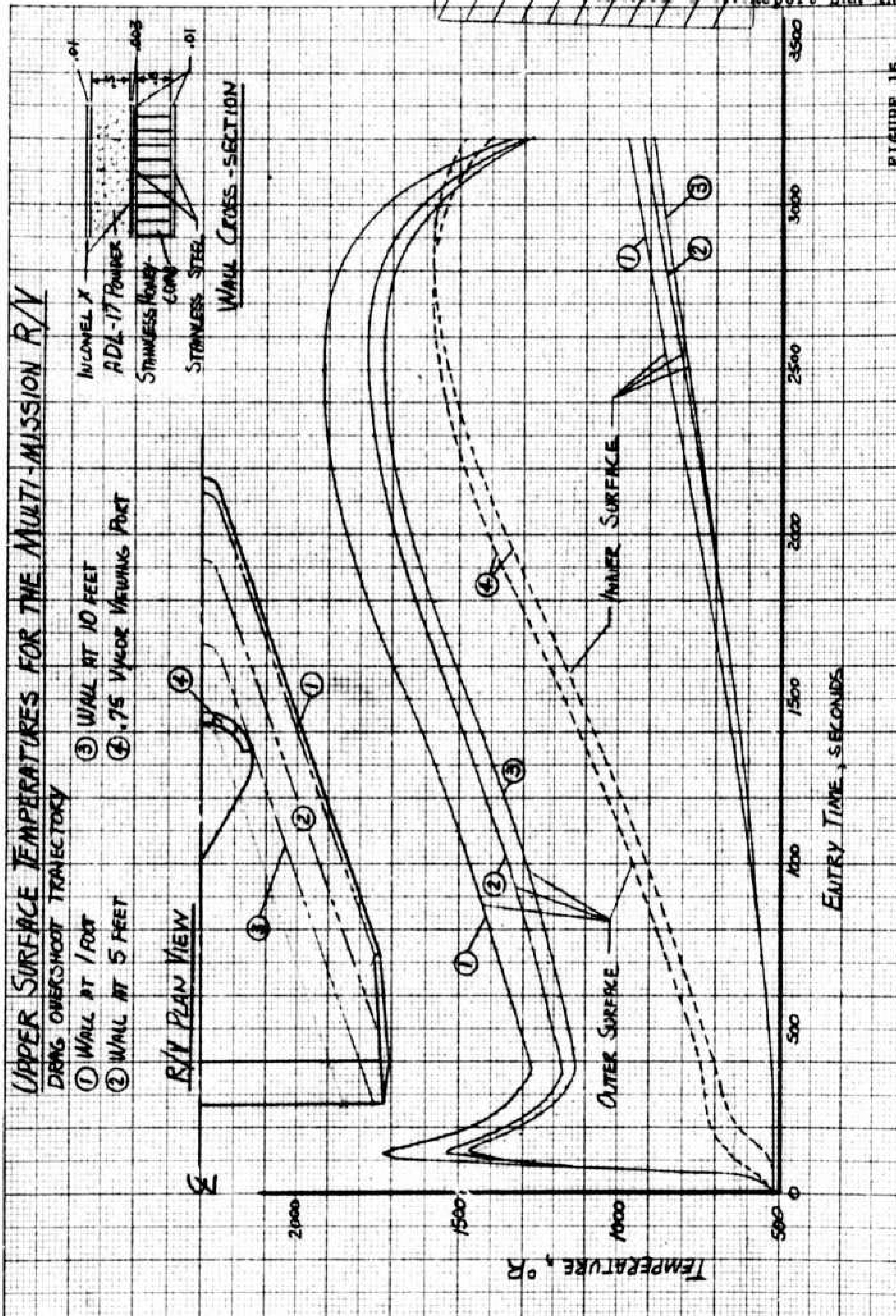

PRIVATE DATA

FIGURE 15